CHEMICAL BONDING AND MÖSSBAUER HYPERFINE INTERACTIONS*

Diana Guenzburger

Centro Brasileiro de Pesquisas Físicas

Rua Xavier Sigaud 150

22290-050 Rio de Janeiro, RJ, Brasil

A historical overview is given of electronic structure calculations of the Mössbauer hyperfine parameters quadrupole splitting, isomer shift and magnetic hyperfine field in molecules and in solids, the latter represented by embedded clusters of atoms. Semi-empirical and first-principles methods based in Density Functional theory were employed. Results are related to characteristics of the chemical bonds.

* Chapter of the book in tribute of Jacques Danon, edited by R. Scorzelli.

I. Introduction

Professor Jacques Danon was a pioneer in establishing a link between the hyperfine parameters measured by Mössbauer spectroscopy and the bonding between the atoms in a solid or a molecule. Ever since the earlier applications of the Mössbauer effect, it became clear that a powerful tool had emerged to probe the distribution of electrons in the systems studied. However, useful information on the chemical bonds could only be extracted with the understanding of the intricate connection between the measured values and the electronic properties. Establishing this connection was, and still is, a very difficult task.

In the early sixties, attempts to interpret the Mössbauer hyperfine parameters had to make use of mostly qualitative concepts, such as covalency, electronegativities, etc. However, self-consistent field (SCF) calculations with the Hartree-Fock method were already available for free atoms and ions, including Fe, the most studied Mössbauer element [1]. Results for these calculations were utilized in the interpretation of the isomer shift δ of componds of Fe. The isomer shift is proportional to the electron density at the nucleus of the probe atom; in the non-relativistic approximation, only s-electrons are found at the nuclear site. By considering the configurations of Fe^{3+} and Fe^{2+} in ionic iron compounds as purely $3d^5$ and $3d^6$, respectively, Walker, Wertheim and Jaccarino (WWJ) [2] derived a calibration for the isomer shift, relating its values to the calculated electron densities of the ions.The difference in the values of the electron density at the nucleus between these two ions is due to differences in shielding of the 3s electrons by the 3d. Danon realized that in a compound the ligand atoms tend to donate electronic charge to the metal ions, especially for higher oxidation states [3]. He therefore modified the WWJ calibration curves by considering for Fe the configuration $3d^54s^{0.32}$, derived from an early Molecular Orbital (MO) calculation, in the complex ion $[FeF_6]^{3-}$, where Fe is in the formal oxidation state +3. The isomer shift of this complex was taken together with that of some ionic compounds of Fe^{2+}, considered to have the configuration $3d^64s^0$. This procedure resulted in a significant

reduction of the magnitude of the WWJ calibration constant; furthermore, the fitting of other Fe compounds into the calibration curves revealed considerable covalency effects, such as nonnegligible 4s populations and charge transfer from the ligands into the 3d orbital.

Another hyperfine property, the quadrupole splitting, is related to the anysotropy of the charge distribution around the probe atom. Danon realized that important information could be obtained from this parameter about the bonding of a metal atom by relating its values to the charge transfer to or from the ligands [4]. Different ligands surrounding a metal atom will create a non-spherical electronic charge distribution that will generate an electric field gradient, and thus a quadrupole splitting.

The magnetic hyperfine field is related to the spin polarization of the s shells. Much chemical information may be gained by understanding the origins of the field, especially the contribution of the valence (n+1)s shell (4s in Fe), which is strongly delocalized .

The development of Quantum Chemical methods that followed made it possible to quantify many of these ideas . Semi-empirical MO methods applied to transition metal complexes, and later more precise methods based on the local density approximation (LDA) of Density Functional (DF) theory, allowed to calculate with increasingly better precision the hyperfine parameters.

In what follows, a brief description will be given of a few calculations , in some of which Danon participated, of hyperfine parameters for systems ranging from transition metal complexes to metallic systems, obtained with electronic structure methods. In all cases , an important outcome of the calculations is the relation between the values obtained and the characteristics of the chemical bond established by the probe atom.

2. Quadrupole Splittings of Ruthenium Complexes

The isotope ^{99}Ru is useful for Mössbauer spectroscopy with the 90 keV transition. A large number of Ru complexes were synthetized and investigated , many of which containing ligands that form strongly covalent bonds with the transition element [5]. Usually this covalency translates into a charge transfer from the ligands to the metal, through the σ bonds. However, some ligands also accept electrons; this occurs when an empty low-energy π orbital is available. This type of charge transfer (metal→ligand π^*) is known as back donation. One of the ligands presenting back donation is nitrosyl (NO) , and it is known to form many complexes with Ru.

Quadrupole splittings obtained in Mössbauer spectroscopy are the consequence of the interaction of non-cubic extranuclear electric fields (electric field gradients) with the nuclear charge density, for nucleus with spin $I > 1/2$, in which case the nucleus has a quadrupole moment $Q \neq 0$. In ^{99}Ru, the splitting observed reflects the energy difference between the sublevels $M_I = \pm 3/2, \pm 1/2$ of the $I=3/2$ excited state of the 90keV transition. In the complex ions investigated [6] $[RuCl_5NO]^{2-}$, $[Ru(NH_3)_5NO]^{2-}$ and $[Ru(CN)_5NO]^{2-}$ (the latter depicted in Fig.1), the presence of the ligand NO lowers the symmetry to C_{4v}, thus generating an electric field gradient at the Ru site. The quadrupole splitting of ^{99}Ru in this symmetry may be expressed as:

$$\Delta EQ = 1/2\ eV_{zz}Q_{3/2} \qquad (1)$$

where V_{zz} is the electric field gradient.

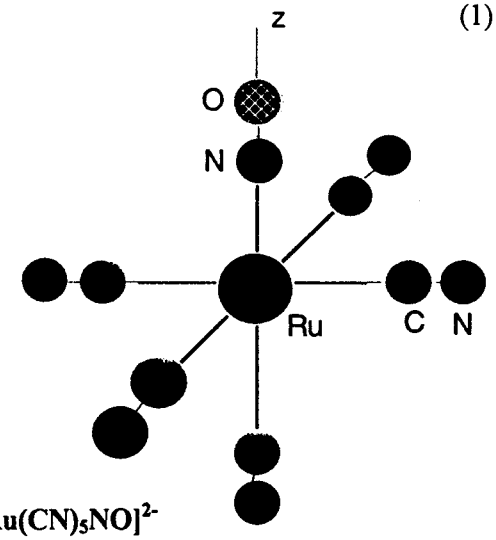

Figure 1. Representation of $[Ru(CN)_5NO]^{2-}$

In covalent complexes such as those studied here, the electric field gradient is dominated by the contribution from the asymmetric electronic charge distribution around the Mössbauer nucleus. Therefore, for complexes with C_{4v} symmetry, within a good approximation V_{zz} may be expressed as:

$$V_{zz} = 4/7\ e\langle r^{-3}\rangle_d [(nd_{x^2-y^2} - nd_{z^2}) + (nd_{xy} - nd_{xz,yz})] \quad (2)$$

if one considers only the 4d orbitals of Ru. In Eq. (2), the terms in parenthesis are the populations (electronic occupations) in the complex of the different d orbitals of Ru , and $\langle r^{-3}\rangle_d$ is the mean value of r^{-3} calculated with the 4d radial function, obtained with atomic Hartree-Fock calculations.

This is actually a simple model for the electric field gradient, in which only the orbitals of the metal atom are considered, but it was used with success in the early calculations of field gradients (seventies) for covalent transition complexes such as the present ones.

But how to obtain the populations of the 4d orbitals, necessary for Eq.(2)? For these, electronic structure calculations for the entire complex were needed. The semi-empirical method denominated SCCC [7] (Self-Consistent Charge and Configuration) made possible MO calculations for transition metal complexes in the computers then available. The SCCC method has the same structure of the self-consistent Hartree-Fock method, but the integrals are all approximated by empirical parameters taken from optical spectra, thus resulting in great simplification.

In Table I are given the calculated populations [6], theoretical and experimental quadrupole splittings of Ru complexes containing NO. It is seen from this table that the calculated ΔEQ is positive in all cases and increases along the series. Analysing the populations, we observe that the most significant change along the series is the decrease in the populations of the $d_{xz,yz}$ orbitals. Since these orbitals are involved in π bonding with the NO ligand, a decrease in their population is due to greater back-donation of electrons into the π^* orbital of NO. Thus we conclude that differences in

the quadrupole splittings in these complexes is mainly a consequence of differences in back-donation to the ligand NO.

Table I

Quadrupole Splittings of Ru Complexes

Complex	Populations				ΔEQ (mm/s)[a]	
	d_{z^2}	$d_{x^2-y^2}$	d_{xy}	$d_{xz,yz}$	Calculated[b]	Experiment[c]
$K_2[RuCl_5NO]$	0.820	0.791	2.000	1.873	0.12	0.18±0.02
$[Ru(NH_3)_5NO]Br_3.H_2O$	0.904	0.870	2.000	1.627	0.35	0.37±0.02
$K_2[Ru(CN)_5NO].2H_2O$	0.989	1.059	1.934	1.497	0.41	0.39±0.01

a) $Q(^{99}Ru)$=0 29b

b) From Ref. (6)

c) From Ref. (5)

3. Isomer Shifts of Iron and Tin Compounds

The isomer shift δ measured in Mössbauer spectroscopy is defined as [8]:

$$\delta = 2/3\ e^2\pi Z S'(Z)\Delta\langle r^2\rangle\ [\rho_A(0) - \rho_S(0)] \equiv \alpha\Delta\rho(0) \qquad (3)$$

where $\Delta\langle r^2\rangle$ is the variation of the mean square radius of the nucleus between the excited and ground states in the Mössbauer transition, S'(Z) is a correction for relativistic effects, and the term in brackets is the difference between the electron density at the nucleus in the absorber A and source S (in other words, between a given

compound and a standard system). As defined, δ is linear against $\rho(0)$ for a series of compounds of the same isotope.

The constant α in Eq. (3) is called the calibration constant. To determine α, a joint effort must be made to associate the electronic term in brackets with experimental values of δ. However, this effort is quite worthwhile since, once α is known, the measurement of the isomer shift of a new compound of the same element will allow to place it in the calibration curve, and thus gain information on the ionic state, covalency, etc . Furthermore, the nuclear constant $\langle r^2 \rangle$ is determined.

A lot of work has been dedicated to determine α for the most common Mössbauer isotopes. After the semi-qualitative calibration curves of WWJ for ^{57}Fe cited in the Introduction, theoretical efforts have been put forth to determine the electron densities in Eq. (3) by electronic structure calculations. This task was challenging due to the presence of heavy atoms; however, in the early seventies new methods based on the Local Density approximation (LDA) were devised which permitted to calculate electron densities from first principles, i.e., without any empirical approximations. One of these methods was the self-consistent Multiple Scattering (known as MS-Xα) [9] , in which the Kohn-Sham equations [10] are solved for a molecule or a cluster of atoms representing a solid, within the muffin-tin approximation for the potential. In the latter, the potential is spherically averaged inside spheres centered at the atomic nuclei and is constant elsewhere in the molecular or cluster region. The Xα local exchange potential [11] was employed.

MS-Xα calculations were performed for the Fe complex ions $[Fe(CN)_6]^{4-}$ [12] , $[Fe(CN)_6]^{3-}$ [13] , FeO_4^{2-} [14] , FeF_6^{3-} , FeF_6^{4-} and FeF_6^{5-} [15] and the value of $\rho(0)$ determined. The plot of δ against $\rho(0) \equiv |\psi(0)|^2$ is shown in Fig. (2); from the line drawn, the value of α of ^{57}Fe is -0.29 mm/s.a_0^{-3}. The two different values for FeF_6^{3-} and FeF_6^{4-} are due to different choices of the muffin-tin radii; in the case of the CN complexes, the choices are much more limited due to the small C-N distance.

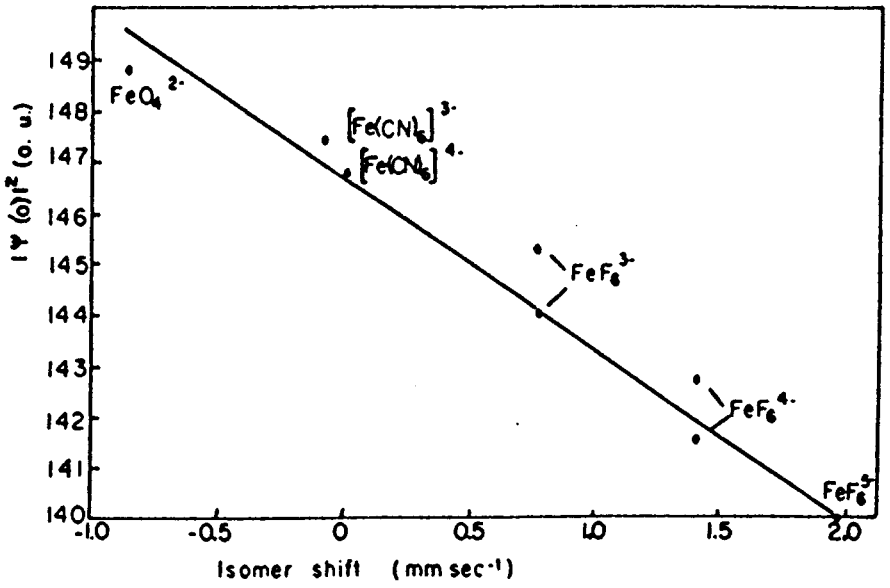

Figure 2

Values of $|\psi(0)|^2$ (1s and 2s orbitals excluded) against isomer shifts of ^{57}Fe. From ref (14). See refs. (12)-(15) for references to experimentel values.

In Table II are given the 3s and valence contributions to $\rho(0)$ for all Fe compunds in Fig.(1). It can be seen that the largest differences in $\rho(0)$ among the compounds come from the valence (4s) contributions. In other words, compounds have lower values of δ mainly if the ligands have a stronger capacity to donate electrons into the Fe 4s orbital via σ bonds.

Table II

Electron densities at the nucleus for Fe componds (in a_0^{-3}) [a)]

	FeF_6^{5-}	FeF_6^{4-}	FeF_6^{3-}	$[Fe(CN)_6]^{4-}$	$[Fe(CN)_6]^{3-}$	FeO_4^{2-}
3s	138.73	139.63	140.60	140.45	140.51	141.17
valence (4s)	1.30	1.93	3.17	6.40	6.94	7.49
Total	140.03	141.56	143.77	146.85	147.45	148.66

a) From refs. (12)-(15) .

The isotope ^{119}Sn is also largely used in Mössbauer spectroscopy, and, more recently, an investigation was carried out with self-consistent first-principles electronic structure calculations for many Sn compunds [16)], represented by clusters with as many as 27 atoms. The method employed was the first principles Discrete Variational (DVM) [17)] , also in the framework of the LDA approximation to Density Functional theory. In the DV method the cluster or molecular orbitals are expanded as a linear combination of numerical atomic orbitals, and the Kohn-Sham equations are solved numerically in a three-dimensional point grid. No muffin-tin approximation to the potential is used; an embedding scheme is employed to account for the external potential of the clusters in the solid. The exchange-correlation potential of von Barth-Hedin [10)] was utilized.

In Fig (3) are plotted the values of δ against $\rho(0)$ for the calculated compounds, in which Sn is in the formal oxidation states +2 and +4. Contrary to ^{57}Fe , the calibration constant of ^{119}Sn is positive: the value of $\langle r^2 \rangle$ derived is $(6.61 \pm 0.58) \times 10^{-3}$ fm^2 .

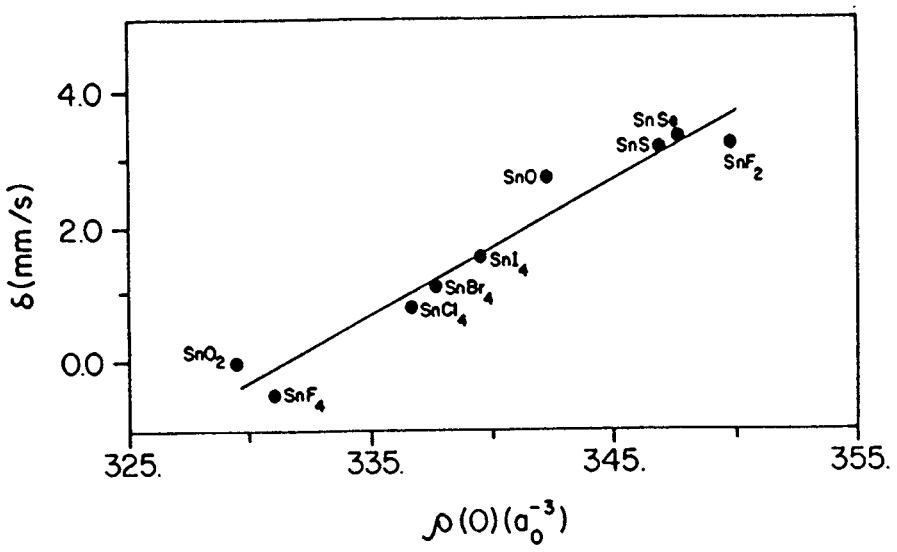

Figure 3

Correlation between δ and ρ(0) (1s, 2s and 3s orbitals excluded) for Sn compounds. From ref.(16).

Lower values of ρ(0) (and thus δ) correspond to compounds of Sn^{4+}, higher values to Sn^{2+}; this is due to the presence in the latter of a lone pair of electrons that contribute strongly to the valence electron density at the nucleus of the metal. Among the compounds in each of the two groups, values of ρ(0) correlate strongly with the electronegativity of the ligands (except SnF_2) . In fact, ligands with large values of the electronegativity attract electrons more efficiently, and thus deplete the 5s orbital of Sn decreasing ρ(0).

4. Magnetism and Field Gradient in Ordered FeNi

One of the many interests of Danon was in meteorites. These fascinating objects that arrive from the cosmos may contain in their body materials not found on earth. This is the case of the ordered compound FeNi known as tetrataenite[18], which crystallizes in the CuAu structure, consisting of alternating layers of Ni and Fe on an fcc lattice. Since this intermetallic compund is magnetic, the existence of an internal magnetic field results in a dependence of the ^{57}Fe quadrupole splitting on the angle θ between the direction of the internal magnetic field and the principal axis of the field gradient [8]:

$$\Delta EQ = 1/2\ eV_{zz}Q_{3/2}\ (3\cos^2\theta - 1)/2 \qquad (4)$$

θ cannot be determined from a single Mössbauer experiment; however , one may calculate V_{zz} at an Fe nucleus from a first-principles calculation using the expression:

$$V_{zz} = -e \int \rho(\mathbf{r})\ (3z^2 - r^2)/r^5\ d\tau + \Sigma_q\ e\ Z^e_q\ (3z^2_q - r^2_q)/r^5_q \qquad (5)$$

where the first term is the electronic contribution obtained with the cluster ρ, and the second term the point-charge contribution of the surrounding nuclei q shielded by the core electrons, with effective charge Z^e_q .Combining the calculated V_{zz} with the measured ΔEQ, the angle θ may be determined.

Spin-polarized DVM calculations were performed [19] for a 19-atom embedded cluster centered on Fe (see Fig.(4)), and the field gradient at this atom obtained according to Eq. (5). The value found for V_{zz} is +0.652 a.u. This result indicates that $\theta=0$ (and not $\theta=90^0$) , that is, the axis of V_{zz} is parallel to the axis of the internal magnetic field, since the measured ΔEQ is also positive. This also implies that the internal magnetic field is oriented perpendicular to the Fe and Ni layers, i.e., along the z axis of Fig. (4). This is an example of a fruitful collaboration between theory and experiment, in which a first-principles calculation provided a result which is very difficult or impossible to obtain in the laboratory.

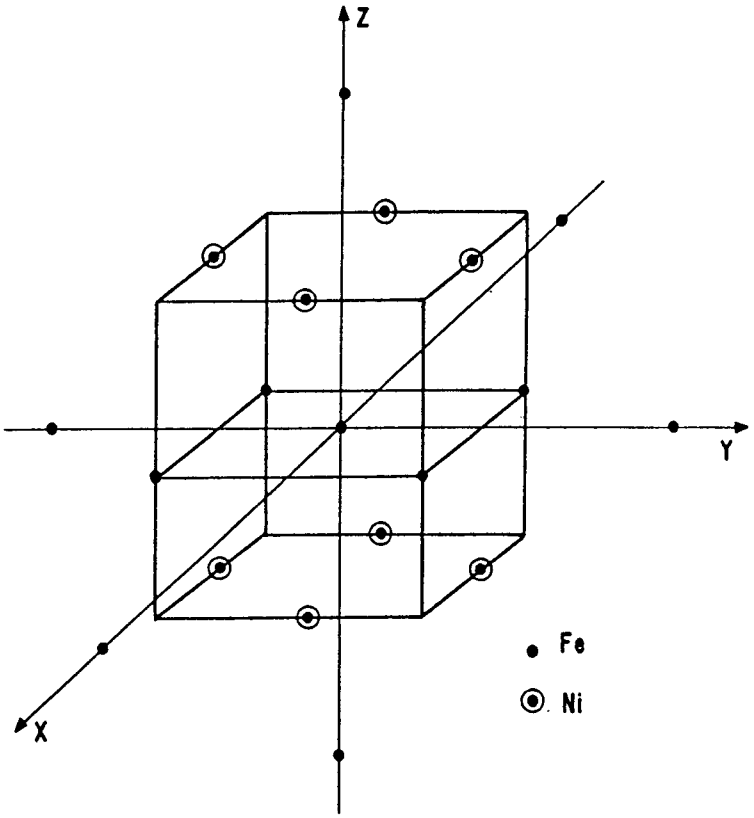

Figure 4

Cluster representing FeNi

Analysing the different contributions to V_{zz}, it was verified that by far the largest came from the spin-down orbitals. This is not surprising since these orbitals are more diffuse than their spin-up counterparts, and thus participate more in bonding. Upon decomposition of the spin-down orbitals V_{zz} into the contributions due to the different symmetries of the D_{4h} point group (see Table III) , we can see that by far the largest contribution comes from the smaller value of the e_g symmetry, contaning the orbitals of Fe $3d_{xz,yz}$, with respect to its partner b_{2g} , containing $3d_{xy}$. This result may again be

explained in terms of bonding. In fact, the e_g orbitals of Fe point towards the Ni atoms in the planes above and below (see Fig (4)), whereas the b_{2g} point towards Fe atoms on the same plane. Since the electronegativity of Ni in a metallic bond is slightly higher than Fe [20], the Ni atoms withdraw some charge from the Fe $d_{xz,yz}$ orbitals (as may be seen from the net Ni charge −0.12 obtained in the population analysis), thus decreasing its contibution to V_{zz}.

Table III

Spin-down Contributions to V_{zz} for FeNi (in a. u.)

3d	
a_{1g} $(3d_z^2)$	−0.680
b_{1g} $(3d_{x^2-y^2})$	+0.681
b_{2g} $(3d_{xy})$	+1.005
e_g $(3d_{xz} + 3d_{yz})$	−0.646
4p	
a_{2u} $(4p_z)$	−0.120
e_u $(4p_x + 4p_y)$	+0.171

5. Magnetic Hyperfine Fields of γ-Fe

Pure bulk iron in the fcc crystal structure (γ-Fe) only exists at very high temperatures (between 1183 and 1667K). However, γ-Fe may be stabilized at low

temperatures as small coherent precipitates in copper or copper-alloy matrices or as thin epitaxial films on a Cu or Cu-based alloy substrate [21), 22)] . Recently the interest in γ-Fe has been revived due to the existence of multiple magnetic states revealed by band-structure calculations [23)] , which is believed to be related to INVAR phenomena in γ-Fe-based alloys.

Recently, spin-polarized DVM calculations were performed for a 62-atom embedded cluster of cubic geometry representing fcc Fe [24)] , for both ferromagnetic (FM) and antiferromagnetic (AFM) spin states, at several lattice constants. For the AFM configuration, a layered arrangements of up and down spins (illustrated in Fig. (5)) was considered.

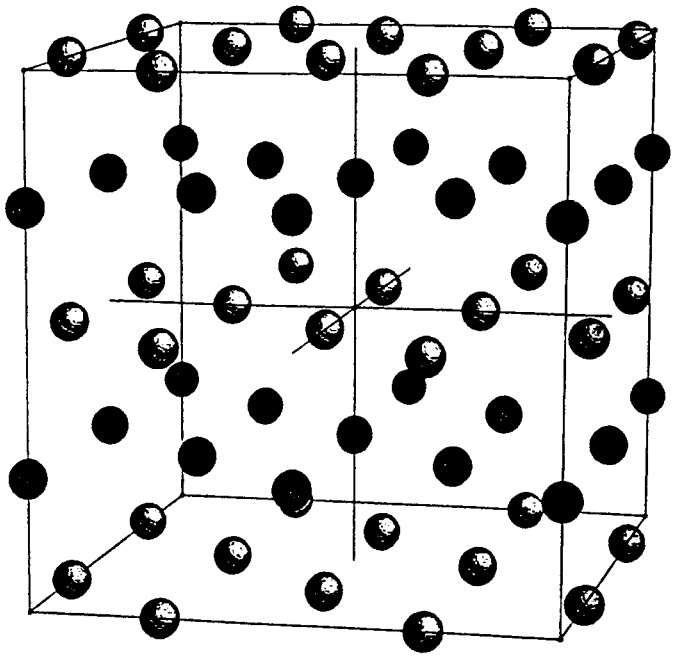

Figure 5

62-atom representation of γ-Fe. Lighter and darker shades stand for spin up and spin down in AFM state.

Measurements of the magnitude of the magnetic hyperfine fields by Mössbauer spectroscopy revealed small values at small interatomic distances and much larger

values at larger distances (see Fig. (6)) [22] .This was ascribed to a large difference in the magnetic moment between AFM γ-Fe, more stable at small lattice constants, and FM γ-Fe, more stable at large lattice constants [23] .

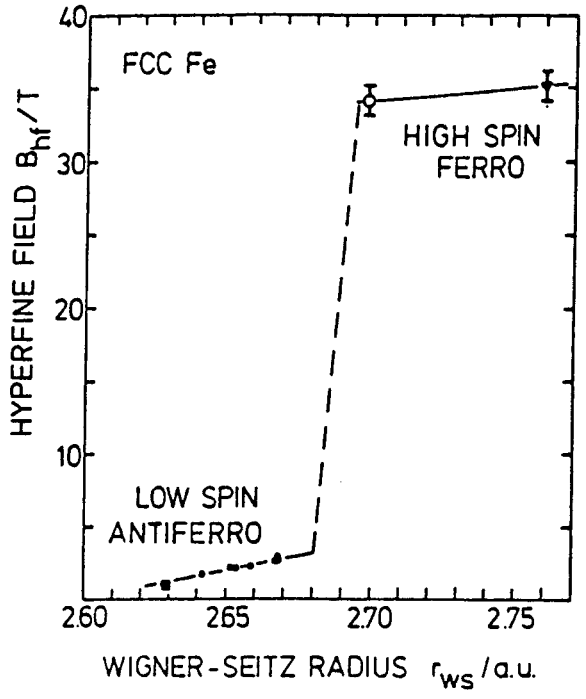

Figure 6

Experimental values of the magnitude of the hyperfine field of fcc Fe at several lattice constants. From ref. (22).

The hyperfine field in metals is constituted mainly of the Fermi or contact field given by:

$$H = 8\pi/3\ \mu_B\ [\rho\uparrow(0)-\rho\downarrow(0)] \qquad (6)$$

where μ_B is the Bohr magneton and the term in parenthesis is the spin density at the nucleus. It is the spin-polarization induced by the Fe spin magnetic moment (mainly 3d) in the s shells that originates the hyperfine field. However, the calculations of the magnetic moments for the two states AFM and FM (Fig. (7)) did not show such a large difference that would justify the large experimental gap in Fig (6).

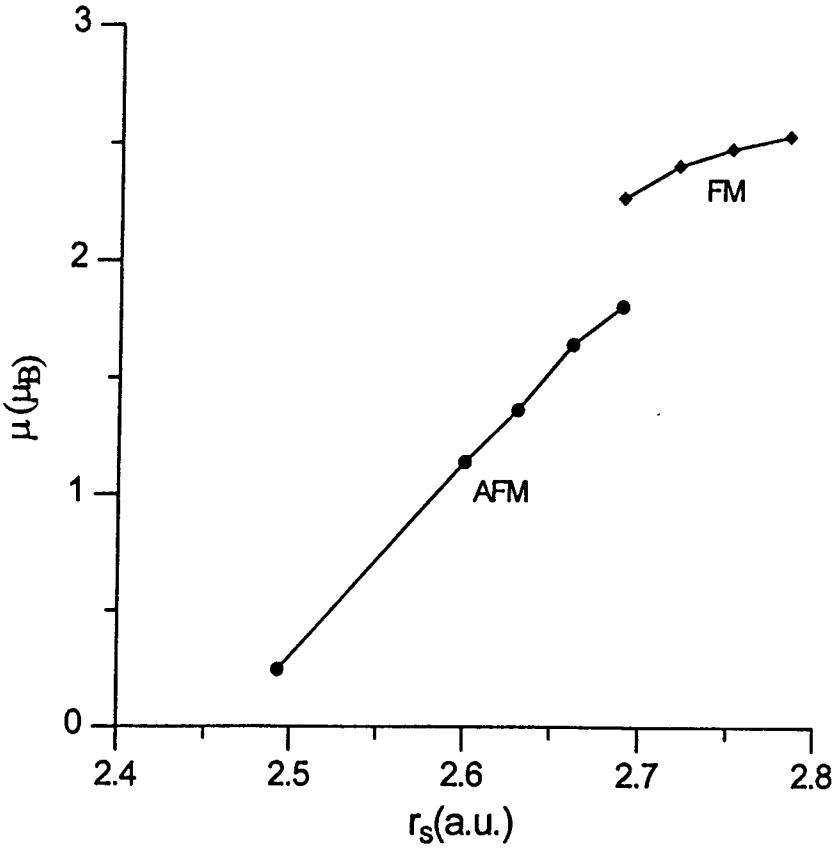

Figure 7

Magnetic moments μ against Wigner-Seitz radius r_s for γ-Fe. From ref (24).

The results of calculations of the hyperfine field according to Eq. (6), displayed in Fig. (8), reveal that the large difference observed experimentally in the magnitude of the hyperfine fields of AFM and FM γ-Fe originates mainly from different signs of the valence electron contribution (4s), which is positive for AFM and negative for FM, and not from large differences in the Fe magnetic moment in the two states. This result shows clearly that the common practice of considering the hyperfine field as proportional to the magnetic moment may be very misleading.

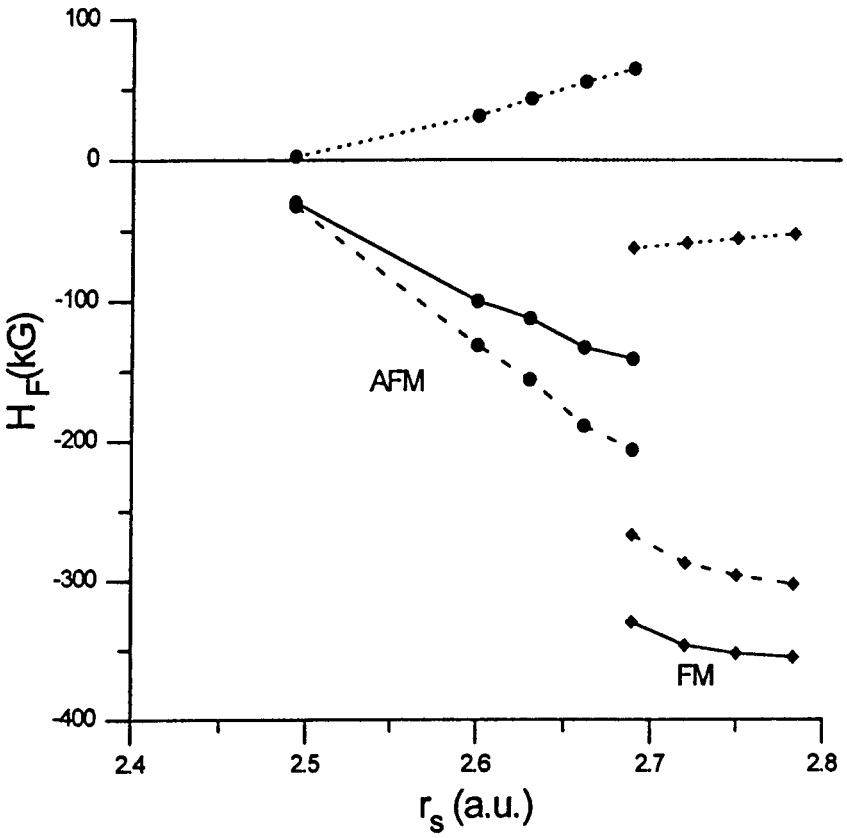

Figure 8

Hyperfine fields H_F against Wigner-Seitz radius r_s for γ-Fe. Core:– – – – – ; valence: .....; total: ———. From ref. (24).

Acknowledgments

The author is thankful to Jacques Danon (in memoriam), for the inspiration that led into this fascinating field of research.

Calculations were performed in part at the Cray Y-MP of the Supercomputing Center of the Universidade Federal do Rio Grande do Sul, Brasiil

References

1) R. E. Watson, Phys. Rev. **118**, 1036 (1960); **119**, 1934 (1960).

2) L. R. Walker, G. K. Wertheim and V. Jaccarino, Phys. Rev. Letters **6**, 98 (1961).

3) J. Danon, "Applications of the Mössbauer Effect in Chemistry and Solid-State Physics", Int. Atomic Energy Agency, Vienna (1966).

4) J. Danon, J. Chem. Phys. **39**, 236 (1963); J. Danon, J. Chem. Phys. **41**, 3378 (1964).

5) W. Potzel, F. E. Wagner, U. Zahn, R. L. Mössbauer and J. Danon, Z. Phys. **240**, 306 (1970).

6) D. Guenzburger, A. Garnier and J. Danon, Inorg. Chim. Acta **21**, 119 (1977).

7) C. J. Ballhausen and H. B. Gray, "Molecular Orbital Theory", Benjamin, New York (1965).

8) N. N. Greenwood and T. C. Gibb, "Mössbauer Spectroscopy", Chapman and Hall, London (1971).

9) K. Johnson, Adv. Quant. Chem. **7**, 143 (1973); J. C. Slater and K. H. Johnson, Phys. Rev. B **5**, 844 (1972).

10) See, for example: R. G. Parr and W. Yang, "Density Functional Theory of Atoms and Molecules", Oxford University Press, New York (1989).

11) J. C. Slater, "Quantum Theory of Molecules and Solids" vol. 4, McGraw-Hill, New York (1974).

12) D. Guenzburger, B. Maffeo and M. L. de Siqueira, J. Phys. Chem. Solids **38**, 35 (1977).

13) D. Guenzburger, B. Maffeo and S. Larsson, Int. J. Quant. Chem. **12**, 383 (1977).

14) D. Guenzburger, D. M. S. Esquivel and J. Danon, Phys. Rev. B **18**, 4561 (1978).

15) M. L. de Siqueira, S. Larsson and J. W. D. Connolly, J. Phys. Chem. Solids **36**, 1419 (1975).

16) J. Terra and D. Guenzburger, J. Phys.: Condens. Matter **3**, 6763 (1991).

17) D. E. Ellis, Int. J. Quant. Chem. **S2**, 35 (1968); D. E. Ellis and G. S. Painter, Phys. Rev. B **2**, 2887 (1970).

18) J. Danon, R. B. Scorzelli, I. Souza Azevedo, J. Laugier and A. Chamberod, Nature **284**, 537 (1980).

19) D. Guenzburger and D. E. Ellis, Phys. Rev. B **36**, 6971 (1987).

20) R. E. Watson and L. H. Bennett, Phys. Rev. B **18**, 6439 (1978).

21) T. Ezawa, W. A. A. Macedo, U. Glos, W. Keune, K. P. Shletz and U. Kirchbaum, Physica B **161**, 281 (1989).

22) W. Keune, T. Ezawa, W. A. A. Macedo, U. Glos and K. P. Schletz, Physica B **161**, 269 (1989).

23) C. S. Wang, B. M. Klein and H. Krakauer, Phys. Rev. Lett. **54**, 1852 (1985).

24) D. Guenzburger and D. E. Ellis, Phys. Rev. B **51**, 12519 (1995).